Demonstration of catch bonds between an integrin and its ligand

Fang Kong,[1] Andrés J. García,[1,2] A. Paul Mould,[3] Martin J. Humphries,[3] and Cheng Zhu[1,2]

[1]Woodruff School of Mechanical Engineering and [2]Coulter Department of Biomedical Engineering, Georgia Institute of Technology, Atlanta, GA 30332
[3]Wellcome Trust Centre for Cell-Matrix Research, Faculty of Life Sciences, University of Manchester, Manchester M13 9PT, England, UK

Binding of integrins to ligands provides anchorage and signals for the cell, making them prime candidates for mechanosensing molecules. How force regulates integrin–ligand dissociation is unclear. We used atomic force microscopy to measure the force-dependent lifetimes of single bonds between a fibronectin fragment and an integrin $\alpha_5\beta_1$-Fc fusion protein or membrane $\alpha_5\beta_1$. Force prolonged bond lifetimes in the 10–30-pN range, a counterintuitive behavior called catch bonds. Changing cations from Ca^{2+}/Mg^{2+} to Mg^{2+}/EGTA and to Mn^{2+} caused longer lifetime in the same 10–30-pN catch bond region. A truncated $\alpha_5\beta_1$ construct containing the headpiece but not the legs formed longer-lived catch bonds that were not affected by cation changes at forces <30 pN. Binding of monoclonal antibodies that induce the active conformation of the integrin headpiece shifted catch bonds to a lower force range. Thus, catch bond formation appears to involve force-assisted activation of the headpiece but not integrin extension.

Introduction

Integrins are heterodimeric membrane receptors that mediate cell adhesion to ECM or to another cell (Hynes, 2002). Integrin–ligand binding provides transmembrane mechanical links to transmit forces from extracellular contacts to intracellular structures (e.g., the cytoskeleton) and signals for a wide variety of cellular processes. For example, binding of integrin $\alpha_5\beta_1$ to fibronectin (FN) plays an important role in fibroblast spreading and motility (Akiyama et al., 1989), T cell migration (Shimizu et al., 1990), osteoblastic and myogenic proliferation, and differentiation (Garcia et al., 1999). Integrins are often expressed on cells in an inactive, low affinity state with slow on rate and/or fast off rate for ligand binding, but they can be activated to high affinity states with fast on rates and/or slow off rates (Hynes, 2002; Luo et al., 2007). On the cell, integrins are usually activated by inside out signaling. Activation can also be triggered by divalent cations and by binding of activating mAbs to cell surface or purified integrins (Humphries, 2000).

Affinity regulation in integrins is thought to be allosteric (Hynes, 2002; Luo et al., 2007). The overall shape of the integrin molecule is that of a large head region (the headpiece) supported on two long legs. In the low affinity state, integrin legs were observed to have bent knees, which were straightened upon activation (Xiong et al., 2001; Takagi et al., 2002). Therefore, it seems reasonable to speculate that tensile force applied via a bound ligand may induce unbending of the knees, thereby converting the integrin from a low affinity state with short bond lifetimes to a high affinity state with long bond lifetimes (Chigaev et al., 2003; Zhu et al., 2005; Alon and Dustin, 2007; Luo et al., 2007; McEver and Zhu, 2007). Indeed, recent studies have provided experimental support for force-enhanced integrin function (Astrof et al., 2006; Woolf et al., 2007; Friedland et al., 2009). Also, steered molecular dynamics simulations have suggested how force activation of integrin might occur (Jin et al., 2004; Puklin-Faucher et al., 2006).

The counterintuitive behavior in which force prolongs bond lifetimes is called catch bonds, which is in contrast to the ordinary slip bond behavior where force shortens bond lifetimes (Dembo et al., 1988). Catch bonds have been demonstrated in interactions between selectins and ligands (Marshall et al., 2003; Sarangapani et al., 2004), actin and myosin (Guo and Guilford, 2006), FimH receptor and mannose (Yakovenko et al., 2008), and glycoprotein Ibα (GPIbα) and von Willebrand factor (VWF; Yago et al., 2008). However, loading rate-dependent

Correspondence to Cheng Zhu: cheng.zhu@bme.gatech.edu

Abbreviations used in this paper: AFM, atomic force microscopy; FN, fibronectin; GPIbα, glycoprotein Ibα; $m\alpha_5\beta_1$, membrane $\alpha_5\beta_1$; PZT, piezoelectric translator; $tr\alpha_5\beta_1$, truncated $\alpha_5\beta_1$; VWF, von Willebrand factor.

The Rockefeller University Press $30.00
J. Cell Biol. Vol. 185 No. 7 1275–1284
www.jcb.org/cgi/doi/10.1083/jcb.200810002

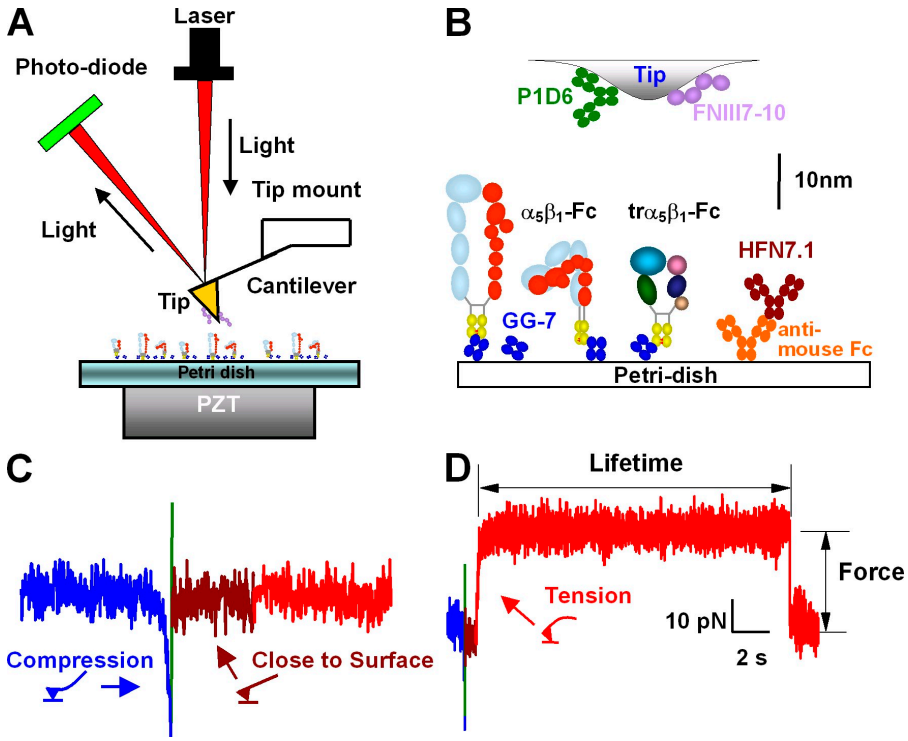

Figure 1. **AFM experiment.** (A) AFM schematic (not to scale) is shown. A laser is focused on the back of cantilever end and bounced onto a photodiode to measure force on the tip that bends the cantilever. A Petri dish is mounted on a PZT with an integrated capacitive sensor to allow for distance control with subnanometer precision. (B) Functionalization of AFM. Molecules depicted represent a composite of several adsorbed or captured on the cantilever tip or the Petri dish. Extended and bent $\alpha_5\beta_1$-Fc, depicted as heterodimers of an α (light blue) and a β (red) subunit fused to an Fc (yellow), and tr$\alpha_5\beta_1$-Fc, consisting of the β propeller (teal) and thigh (dark green) domains of the α subunit as well as the βA (pink), hybrid (dark blue), and plexin/semaphorin/integrin (tan) domains of the β subunit fused to an Fc, were captured by an anti-Fc mAb (GG-7) Fab (blue) preadsorbed on the Petri dish. In some experiments, these were replaced by an anti-FN mAb (HFN7.1; brown) captured by an anti–mouse Fc antibody (orange) preadsorbed on the Petri dish. $FNIII_{7–10}$ (purple) was adsorbed on the cantilever tip. In some control experiments, $FNIII_{7–10}$ was replaced by an anti-$\alpha_5\beta_1$ mAb (P1D6; green). (C) Force-scan trace without adhesion. The Petri dish was moved up by the PZT to contact the cantilever tip (blue trace), immediately retracted to a small distance (green trace) from the tip to reduce nonspecific adhesion, held at this distance for 0.5 s to allow for bond formation (brown trace), and retracted away from the tip to detect adhesion (red trace). The trace illustrates a contact cycle without binding where the retraction curve returned to zero force upon Petri dish retraction. (D) Force-scan trace with adhesion. The color codes are the same as those in C, which illustrates a contact cycle with binding and lifetime measurement. Petri dish retraction resulted in a tensile force indicating binding. Once the pulling force reached a preset value (indicated), a feedback loop was triggered to keep the cantilever deflection at the set point. The lifetime at that force (indicated) was measured until bond failure, signified by the springing back of the cantilever to the level of zero mean force. The bending configurations of the cantilever are depicted with colors matching the corresponding colors of the traces in C and D.

rupture force measurements with atomic force microscopy (AFM) force-ramp experiments and dynamic force spectroscopy analysis have not revealed catch bonds for integrin–ligand interactions (Li et al., 2003; Zhang et al., 2002, 2004), nor did cell tether lifetime measurements with a flow chamber (Vitte et al., 2004).

Using AFM force-clamp experiments, we measured lifetimes of single FN–$\alpha_5\beta_1$ bonds at forces as low as 4 pN. Catch bonds were observed in <30 pN. Changing divalent cations altered lifetimes in the same force range and binding of a mAb that reports the extended conformation of $\alpha_5\beta_1$, but the catch bonds remained. Truncating the $\alpha_5\beta_1$ leg regions further prolonged bond lifetimes and abolished the response of the lifetime versus force curve to divalent cations; nevertheless, catch bonds were still observed, showing that leg extension is not required for catch bonds. Two activating mAbs that bind the headpiece shift catch bonds to a lower force range, indicating that force-induced activation of the headpiece is involved in catch bond formation. Thus, catch bond formation appears to involve force-assisted activation of the headpiece but not integrin extension.

Results

Using AFM (Fig. 1 A), we measured interactions between an FN fragment ($FNIII_{7–10}$ [FN fragment encompassing the 7–10th type III repeats]) and a recombinant $\alpha_5\beta_1$ consisting of either the full extracellular portion ($\alpha_5\beta_1$-Fc) or only the headpiece (truncated $\alpha_5\beta_1$ [tr$\alpha_5\beta_1$]-Fc) fused with Fc (Coe et al., 2001; Mould et al., 2002). We have shown previously that the recombinant proteins closely mimic the function and conformational regulation of the native integrin (Coe et al., 2001; Mould et al., 2002, 2003a,b, 2005). To avoid uncontrolled adsorption of integrin via different domains, which could produce variable results and restrict conformational changes, tr$\alpha_5\beta_1$-Fc was captured by Fab of an anti-Fc mAb (GG-7) preadsorbed on a polystyrene Petri dish (Fig. 1 B). Antibody capture also ensured more uniform integrin orientation. The Petri dish was driven by a piezoelectric translator (PZT) to contact $FNIII_{7–10}$ adsorbed on a cantilever tip (Fig. 1 A). The absence (Fig. 1 C) or presence (Fig. 1 D) of adhesion was detected upon retraction of the PZT, which was then clamped at a desired force for lifetime measurement (Fig. 1 D).

Experiments were performed in 1 mM Ca^{2+} plus 1 mM Mg^{2+} (Ca^{2+}/Mg^{2+}), 2 mM Mg^{2+} plus 2 mM EGTA (Mg^{2+}/EGTA), or 2 mM Mn^{2+} in the absence or presence of blocking or activating mAbs or a competing peptide. At the same GG-7–coating concentrations, binding of $\alpha_5\beta_1$-Fc (Fig. 2 A) or tr$\alpha_5\beta_1$-Fc (Fig. 2 C) to $FNIII_{7–10}$ became progressively more frequent when the cation condition was changed from Ca^{2+}/Mg^{2+} to Mg^{2+}/EGTA and to Mn^{2+}. This was corroborated by flow cytometry data showing that Mg^{2+}/EGTA and Mn^{2+} increased the staining of $\alpha_5\beta_1$-Fc–coated beads by a mAb that reports unbending of the knees (9EG7; Fig. S1), which is consistent with previous experiments (Humphries, 2000). Binding was

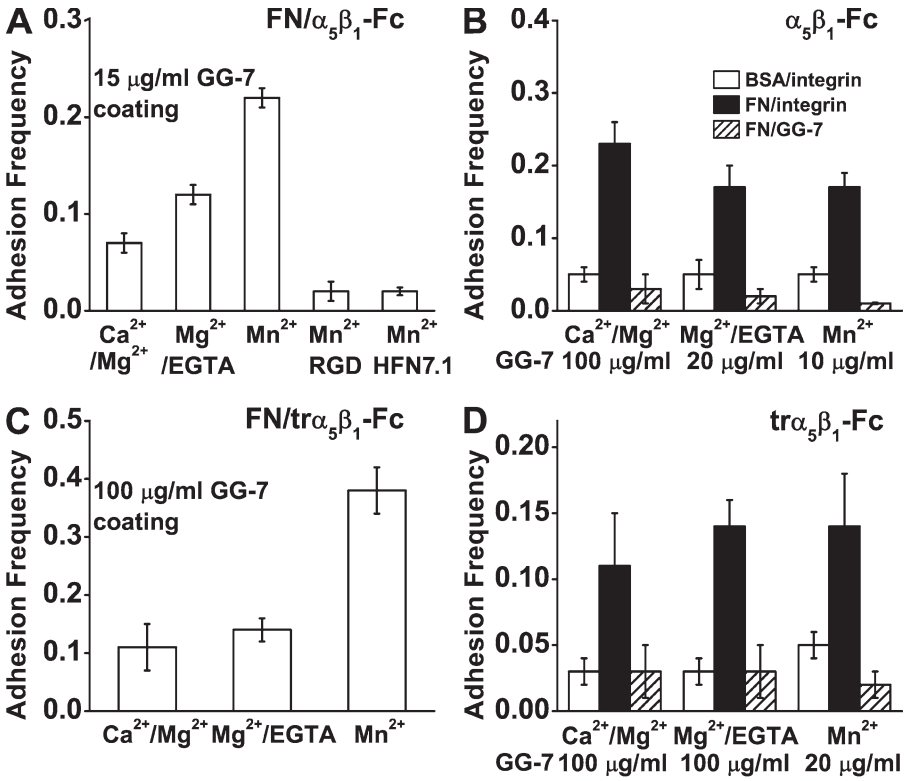

Figure 2. **Binding specificity.** (A and B) $\alpha_5\beta_1$-Fc data are shown. (C and D) tr$\alpha_5\beta_1$-Fc data are shown. Frequencies of adhesion between 10 μg/ml $FNIII_{7–10}$ adsorbed on cantilever tips and 10 μg/ml $\alpha_5\beta_1$-Fc (A) or tr$\alpha_5\beta_1$-Fc (C) captured by 15 or 100 μg/ml GG-7 Fab precoated on Petri dishes in buffer containing the indicated cations without or with cyclo(-GRGDSP) or HFN7.1 in solution were enumerated in 100 tests for each spot and presented as mean ± SEM of 3–5 spots. Frequencies (measured with the same protocol as in A and C) of adhesion between 10 μg/ml $FNIII_{7–10}$ coated on cantilever tips and 10 μg/ml $\alpha_5\beta_1$-Fc (B) or tr$\alpha_5\beta_1$-Fc (D) captured by GG-7 Fab preadsorbed on Petri dishes with indicated concentrations (closed bars) are compared with those between BSA-coated tips and tr$\alpha_5\beta_1$-Fc–functionalized Petri dishes (open bars) and with those between $FNIII_{7–10}$-coated tips and GG-7–coated Petri dishes without incubating with tr$\alpha_5\beta_1$-Fc (hatched bars) in the indicated cation conditions.

specific, as it was abolished by addition to the solution of mAb HFN7.1, which blocked the integrin-binding site in $FNIII_{7–10}$ or an RGD-containing peptide cyclo(-GRGDSP), which competed with the RGD loop in $FNIII_{7–10}$ for $\alpha_5\beta_1$ binding (Fig. 2 A). To maintain infrequent binding (<20%), a requirement for most adhesion events to be mediated by single bonds, progressively lower GG-7–coating concentrations were used for experiments in Ca^{2+}/Mg^{2+}, Mg^{2+}/EGTA, and Mn^{2+} to compensate for the progressively higher binding affinities of tr$\alpha_5\beta_1$-Fc (Fig. 2, B and D). In all three cation conditions, binding was abrogated when the cantilever tips coated with $FNIII_{7–10}$ were switched to those coated with BSA or when the Petri dishes functionalized with integrins were switched to those that were not functionalized (Fig. 2, B and D).

Mechanical regulation of FN–$\alpha_5\beta_1$ dissociation was quantified by the force dependence of mean lifetimes of mostly single $FNIII_{7–10}$–$\alpha_5\beta_1$ bonds measured in each of the three cation conditions (Fig. 3, A–C, circles). As force increased, lifetime first decreased to a minimum, then increased to a maximum, and decreased again, exhibiting a triphasic transition from slip bonds to catch bonds and then to slip bonds again. The first slip bond regimen was most clearly observed in Ca^{2+}/Mg^{2+} (Fig. 3 A) but became less pronounced in Mg^{2+}/EGTA (Fig. 3 B) and Mn^{2+} (Fig. 3 C). The much less frequent nonspecific binding between BSA-coated cantilevers and polystyrene Petri dishes functionalized with $\alpha_5\beta_1$-Fc contributed negligibly to these lifetime versus force curves, as most of these events were ruptured at forces <20 pN (Fig. S2 A), and those that survived the ramping had very short lifetimes (Fig. 3 C, diamonds).

To control for potential artifacts of the chimeric integrin that fuses the extracellular portions of the α_5 and β_1 chains with a human IgG Fc region (Coe et al., 2001), we measured the specific binding (Fig. S2 A) of $FNIII_{7–10}$ to membrane $\alpha_5\beta_1$ (m$\alpha_5\beta_1$) purified from human smooth muscle cells reconstituted in glass-supported lipid bilayers in Mg^{2+}/EGTA. Although the lifetimes were shorter, the force-dependent curve of m$\alpha_5\beta_1$ exhibited the same triphasic pattern (Fig. 3 D) qualitatively similar to the $\alpha_5\beta_1$-Fc curves (Fig. 3, A–C). Thus, catch bonds were observed at forces ranging from 10–30 pN for FN interacting with $\alpha_5\beta_1$-Fc and m$\alpha_5\beta_1$.

Because $\alpha_5\beta_1$-Fc was captured by preadsorbed GG-7, rupture of the molecular complex might result from dissociation of the FN–$\alpha_5\beta_1$ or Fc–GG-7 bond (Fig. 3 E). We neglect potential detachment of $FNIII_{7–10}$ from the cantilever tip or of GG-7 from the Petri dish because physioadsorption of proteins is generally much stronger than specific protein–protein interactions (Rief et al., 1997). To determine the rupture loci, we overlaid the force-dependent lifetimes of directly adsorbed $\alpha_5\beta_1$-Fc interacting with GG-7 (Fig. 3 F) on each panel of Fig. 3 (A–C, squares). Slip bonds were observed over the entire force range tested. The mean lifetimes at forces <25 pN were much longer than those of $FNIII_{7–10}$ interacting with captured $\alpha_5\beta_1$-Fc, indicating that the observed catch bonds were characteristic of the FN–$\alpha_5\beta_1$ bond rather than the Fc–GG-7 bond. However, at forces >30 pN, the black circle curves in Fig. 3 (B and C) became indistinguishable from the gray square curve, suggesting that the second slip bonds of the former curves result from dissociation of the Fc–GG-7 bond rather than the FN–$\alpha_5\beta_1$ bond. Because the dissociation rate of two bonds in series equals to the sum of the two individual dissociation rates, the lifetimes of these two bonds in series would have been significantly shorter than either bond measured separately if lifetime of the FN–$\alpha_5\beta_1$-Fc bond were

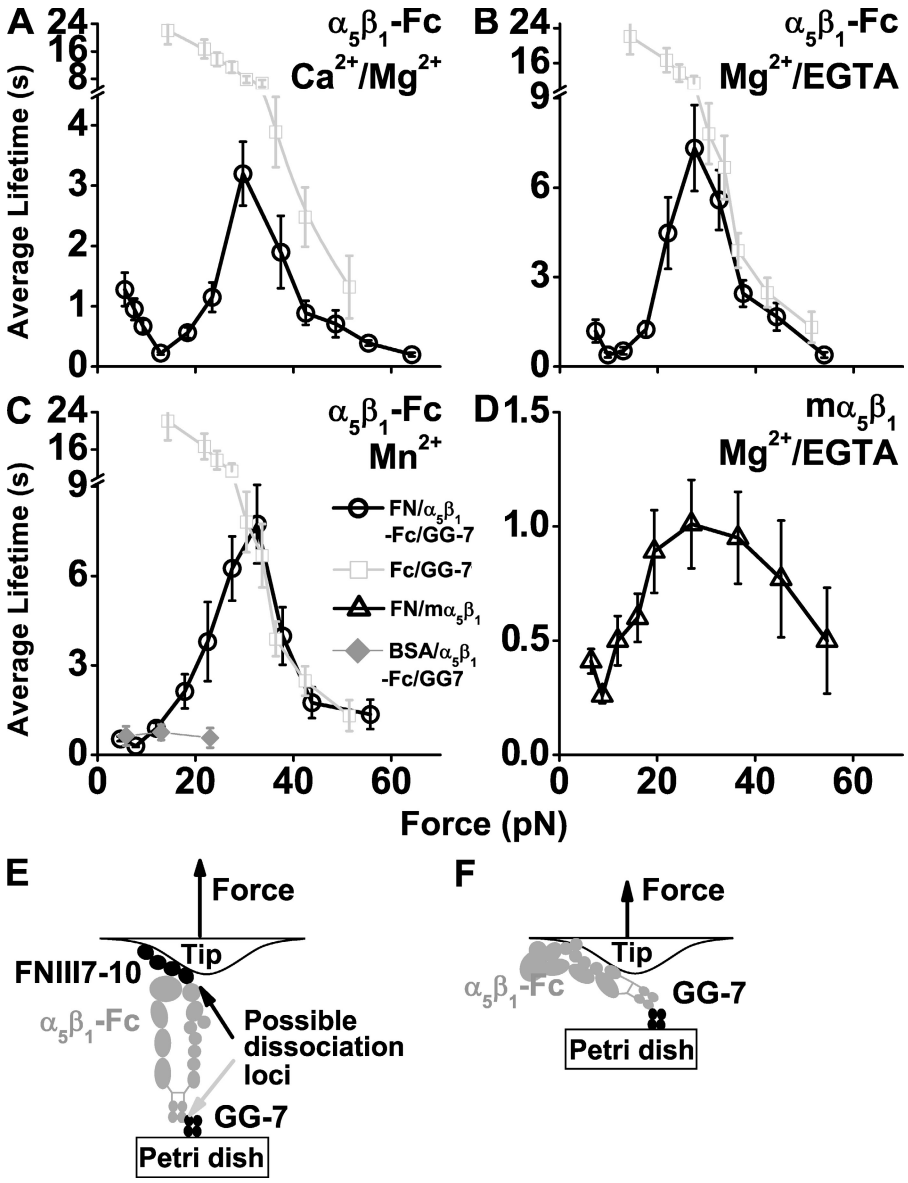

Figure 3. **Lifetimes of FN–$\alpha_5\beta_1$ bonds.** (A–C) Plots of lifetime versus force of $\alpha_5\beta_1$-Fc–functionalized Petri dish dissociating from $FNIII_{7–10}$-coated cantilever tips (circles) in Ca^{2+}/Mg^{2+} (A), Mg^{2+}/EGTA (B), and Mn^{2+} (C). (D) A qualitatively similar plot (triangles) of $m\alpha_5\beta_1$ reconstituted into lipid bilayer dissociating from $FNIII_{7–10}$-coated cantilever tips in Mg^{2+}/EGTA confirmed the catch bond observation. Also plotted in A–C is the lifetime versus force curve of Fc dissociating from GG-7 (squares). For B and C, the black and gray curves overlap at forces >30 pN, indicating that measured lifetimes beyond 30 pN were caused by Fc–GG-7 dissociation instead of $FNIII_{7–10}$–$\alpha_5\beta_1$-Fc dissociation. Also shown in C is a lifetime versus force plot (diamonds) of $\alpha_5\beta_1$-Fc–functionalized Petri dish dissociating from BSA-coated cantilever tips measured in Mn^{2+}. (E) Schematic of the molecular arrangement indicating possible dissociation loci between $FNIII_{7–10}$ and $\alpha_5\beta_1$-Fc or between $\alpha_5\beta_1$-Fc and GG-7. (F) Schematic of the molecular arrangement for experiments that measured the capturing strength of the Fc–GG-7 interaction. Error bars indicate mean ± SEM.

comparable with the Fc–GG-7 bond. The fact that the lifetime versus force curves of the FN–$\alpha_5\beta_1$-Fc–GG-7 and $\alpha_5\beta_1$-Fc–GG-7 bonds were indistinguishable shows that the FN–$\alpha_5\beta_1$ bond lifetimes in Mg^{2+}/EGTA or Mn^{2+} were substantially longer than the Fc–GG-7 bond lifetimes at forces >30 pN. They might continue to behave as catch bonds at forces >30 pN before (and if) it transitioned to slip bonds. In contrast, in Ca^{2+}/Mg^{2+}, the lifetime of the FN–$\alpha_5\beta_1$-Fc–GG-7 serial bonds was significantly shorter than that of the Fc–GG-7 bond in the entire force range (Fig. 3 A). Therefore, the observation of catch slip transition beyond 30 pN is reliable. However, the real differences of FN–$\alpha_5\beta_1$ bond lifetimes between Ca^{2+}/Mg^{2+} and Mg^{2+}/EGTA or Mn^{2+} conditions may be much greater than those apparent in Fig. 3 (A–C).

For comparison, we also measured force-dependent lifetimes of $\alpha_5\beta_1$ and $FNIII_{7–10}$ bound to their respective blocking mAbs, P1D6 and HFN7.1 (Fig. 4, schematics), which were also specific to the antigen–antibody interactions (Fig. S2, C and D). Similar to the Fc–GG-7 interaction and consistent with other antibody–antigen interactions characterized previously (Marshall et al., 2003; Sarangapani et al., 2004), slip bonds were observed in both cases (Fig. 4) as the mean lifetimes decreased monotonically with increasing force in the same range where the triphasic transitions between slip and catch bonds were observed for $\alpha_5\beta_1$ interacting with its physiological ligand (Fig. 3, A–C). Despite their similar slip bond behaviors, the P1D6–$\alpha_5\beta_1$-Fc–GG-7 serial bonds were much longer lived than the anti–mouse antibody–HFN7.1–$FNIII_{7–10}$ serial bonds, especially at low forces (Fig. 4, compare A with B), revealing different interaction characteristics of the different antibody–antigen pairs.

A large percentage of $\alpha_5\beta_1$-Fc appeared to exist in a bent conformation in Ca^{2+}/Mg^{2+}, but more of the integrin became extended in Mg^{2+}/EGTA and Mn^{2+} (Fig. S1; Takagi et al., 2002; Mould et al., 2005; Zhu et al., 2008). Yet in all three cation conditions, lifetimes at low forces (<10 pN) were similarly short (<2 s). As force increased from 10–30 pN, catch bonds were

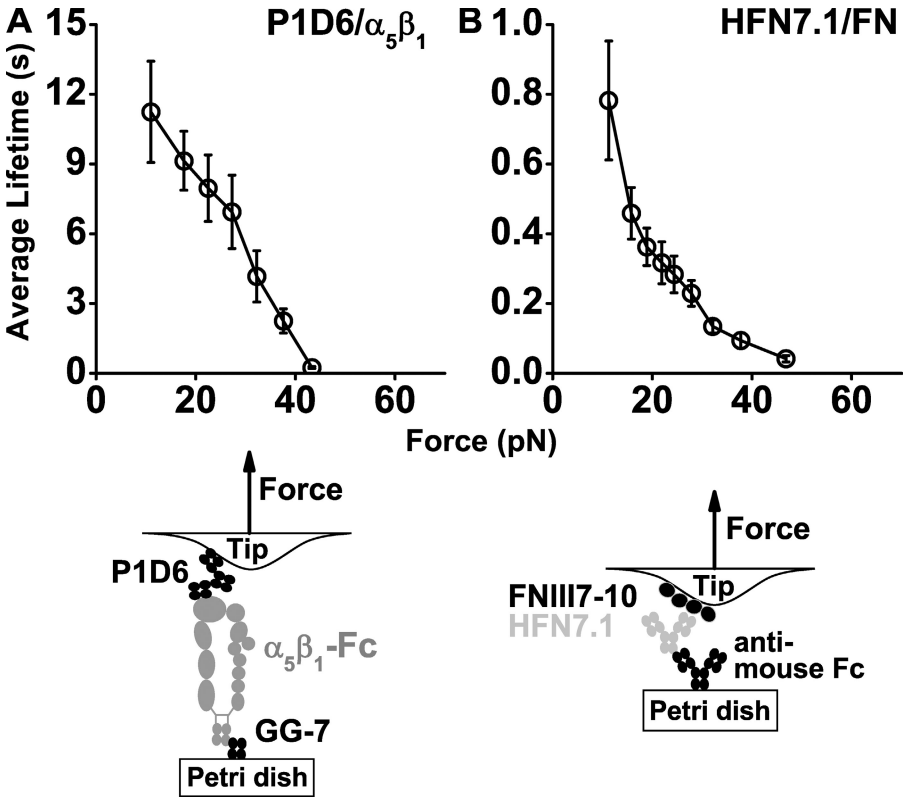

Figure 4. **Lifetimes of antibody–antigen bonds.** (A and B) Plots of lifetime (mean ± SEM) versus force of interactions between $\alpha_5\beta_1$-Fc–functionalized Petri dish and P1D6-coated cantilever tips (A) and between HFN7.1 captured by anti–mouse Fc antibody preadsorbed on Petri dish and $FNIII_{7–10}$-coated cantilever tips (B). Schematics depict the molecular arrangement for the experiments.

observed, but lifetimes were prolonged less by force in Ca^{2+}/Mg^{2+} (Fig. 3 A) than Mg^{2+}/EGTA (Fig. 3 B), which were similar to Mn^{2+} (Fig. 3 C). These data indicate that catch bonds may not result from a force-induced unbending of the integrin. To obtain more definitive evidence, we repeated the experiments shown in Fig. 3 (A–C) using tr$\alpha_5\beta_1$-Fc that contains only a five-domain headpiece of the integrin fused with Fc (Coe et al., 2001; Mould et al., 2002). As anticipated, catch bonds were still observed, confirming that the integrin legs and the unbending conformational change were not required for the FN–$\alpha_5\beta_1$ catch bonds (Fig. 5, A–C). Interestingly, in the ~10–25-pN range, truncating the integrin leg regions enabled force to prolong lifetimes to a greater extent than the integrin with legs (Fig. 5, compare circles with triangles replotted from Fig. 3). The lifetime versus force curves in the catch bond regimen were quite similar for all three cation conditions (compare Fig. 5, A–C). However, similar to the $FNIII_{7–10}$–$\alpha_5\beta_1$ case, the force where the $FNIII_{7–10}$–tr$\alpha_5\beta_1$ catch bonds might transition to slip bonds could not be determined, for the mean lifetimes of the $FNIII_{7–10}$–tr$\alpha_5\beta_1$-Fc–CG-7 serial bonds coincided with the Fc–GG-7 bond at a force >25 pN in all three cation conditions (Fig. 5, A–C, compare black circles and gray squares replotted from Fig. 3), indicating that these represented lifetimes of the Fc–GG-7 bond rather than the $FNIII_{7–10}$–tr$\alpha_5\beta_1$-Fc bond.

To explore the structural mechanism of the observed catch bonds, we measured $FNIII_{7–10}$–$\alpha_5\beta_1$-Fc bond lifetimes in Mn^{2+} in the presence of TS2/16 (Fig. 6 A) or 12G10 (Fig. 6 B). These two mAbs bind to the βA domain (Fig. 6 D, schematic) to further activate integrins by shifting or stabilizing the position of the α1 helix known to be critical for integrin activation (Mould et al., 2002; Xiao et al., 2004). Both mAbs left shifted the catch bond region, but TS2/16 yielded longer lifetimes at low forces (Fig. 6 A) compared with 12G10 (Fig. 6 B). Interestingly, TS2/16 also left shifted the $FNIII_{7–10}$–tr$\alpha_5\beta_1$-Fc catch bond region but did not prolong lifetimes as much as it did for the $FNIII_{7–10}$–$\alpha_5\beta_1$-Fc case (Fig. 6 C). Use of activating antibodies also exposed a slip bond region (Fig. 6, A–C). These data emphasize the importance of the βA domain α1 helix and link the $FNIII_{7–10}$–tr$\alpha_5\beta_1$ catch bonds to $\alpha_5\beta_1$ activation.

Discussion

Catch bonds represent unusual, counterintuitive behaviors that have recently been observed in selectin–ligand (Marshall et al., 2003; Sarangapani et al., 2004), actin–myosin (Guo and Guilford, 2006), FimH–mannose (Yakovenko et al., 2008), and GPIbα–VWF (Yago et al., 2008) interactions. Based on the integrin structures and their conformational change models, it has been speculated that integrin–ligand interactions may also behave as catch bonds (Chigaev et al., 2003; Zhu et al., 2005; Alon and Dustin, 2007; Luo et al., 2007; McEver and Zhu, 2007). However, published work did not observe integrin–ligand catch bonds (Zhang et al., 2002, 2004; Li et al., 2003). In the previous work, force-ramp experiments were used to measure ramp rate-dependent rupture forces, which were analyzed by dynamic force spectroscopy, assuming that dissociation occurs along a single pathway and off rate increases exponentially with increasing force as modeled by Bell (1978), which precluded catch bonds. Using AFM force-clamp experiments, we observed triphasic force-dependent bond lifetimes that

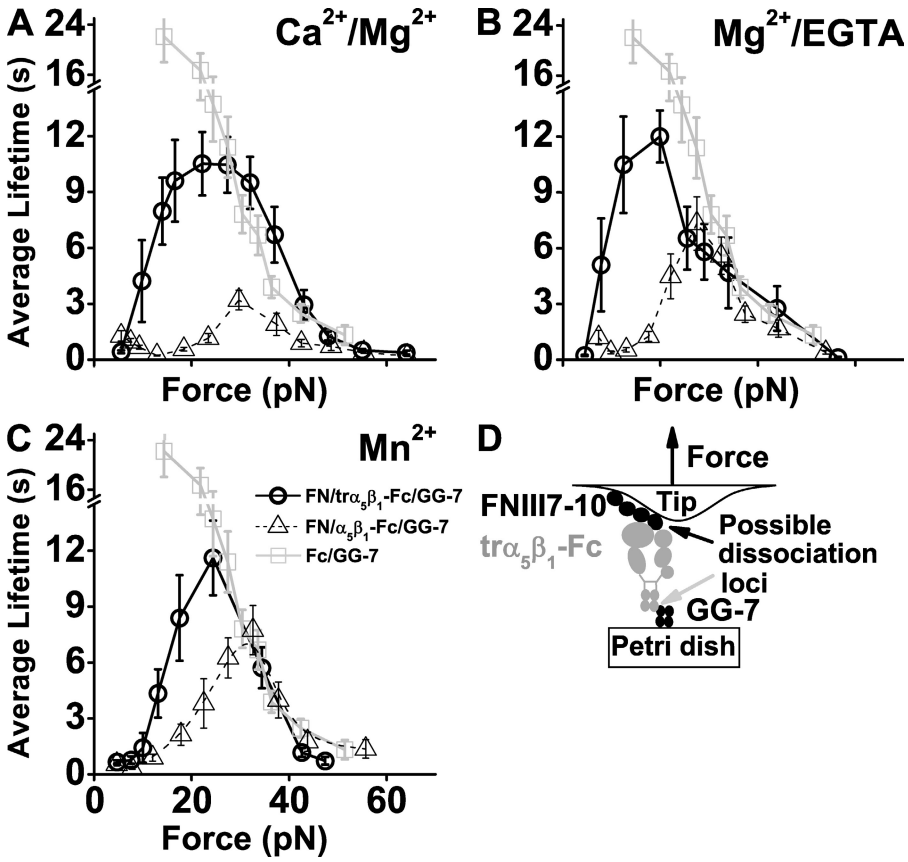

Figure 5. **Lifetimes of FN–tr$\alpha_5\beta_1$ bonds.** (A–C) Plots of lifetime (mean ± SEM) versus force of tr$\alpha_5\beta_1$-Fc–functionalized Petri dish dissociating from $FNIII_{7–10}$-coated cantilever tips (circles) in Ca^{2+}/Mg^{2+} (A), Mg^{2+}/EGTA (B), and Mn^{2+} (C). Data from Fig. 3 (A–C) are replotted in A–C for comparison. The lifetime versus force curves of $\alpha_5\beta_1$-Fc–functionalized Petri dish dissociating from $FNIII_{7–10}$-coated cantilever tips are shown as triangles, and $\alpha_5\beta_1$-Fc–coated cantilever tips dissociating from GG-7–functionalized Petri dish are shown as squares. (D) Schematic of the molecular arrangement indicating possible dissociation loci between $FNIII_{7–10}$ and tr$\alpha_5\beta_1$-Fc or between tr$\alpha_5\beta_1$-Fc and GG-7.

deviate from the Bell model, demonstrating FN–$\alpha_5\beta_1$ catch bonds (Figs. 3, 5, and 6).

It is known that integrin-mediated adhesion can be strengthened by integrin clustering or binding of multiple integrins cooperatively, which can be induced by force (Galbraith et al., 2002). However, this is unlikely the mechanism for the observed catch bonds for the following reasons. First, (tr)$\alpha_5\beta_1$-Fc molecules were captured by GG-7 Fab, which was unlikely to adsorb on Petri dishes as clusters. Nor was the $FNIII_{7–10}$ likely to adsorb on AFM tips as clusters. Without preclustering, without active cellular mechanisms to cluster the molecules, and without lateral mobility, it is unlikely that integrins bind in clusters in our experiments. Second, using the same AFM setup in the control experiments, we observed only slip bonds for the $\alpha_5\beta_1$-Fc–GG-7 (Fig. 3), P1D6–$\alpha_5\beta_1$-Fc–GG-7 (Fig. 4 A), and $FNIII_{7–10}$–HFN7.1–anti–mouse Fc (Fig. 4 B) interactions. Slip bonds were observed in these cases despite that the $\alpha_5\beta_1$-Fc–GG-7 interaction was monomeric (because Fab was used; Fig. 3 F), P1D6–$\alpha_5\beta_1$-Fc–GG-7 interaction might be dimeric (because whole P1D6 was used; Fig. 3 A, schematic), and $FNIII_{7–10}$–HFN7.1–anti–mouse Fc interaction might be multimeric (because whole HFN7.1 and anti–mouse Fc were used; Fig. 3 B, schematic). Third, we examined the correlation of (or the lack thereof) bond lifetime with molecular stiffness (Fig. S3 A). We have previously shown that the stiffness of multiple bonds is multiple times of that of a single bond (Sarangapani, 2005), which predicts a positive correlation between lifetime and stiffness if the longer lifetimes were caused by greater bond multiplicity. However, such correlation was not observed (Fig. S3, A and B). To the contrary, the mean stiffness values for molecular complexes that had lifetimes clustered around 0.3, 2.8, and 10 s are indistinguishable from each other (Fig. S3 C). These data ruled out higher multiplicity of bonds as the cause for longer lifetimes at high forces than the lifetimes at low forces in the catch bond regime. Finally, we have previously shown that formation of dimeric bonds cannot generate catch bonds if the corresponding monomeric interaction is a slip bond. The effects of dimeric bonds are to shift the lifetime versus force curve of the monomeric bond rightward toward doubling the force and upward toward doubling the lifetime (Marshall et al., 2003).

Our flow cytometry data suggest that more $\alpha_5\beta_1$-Fc became extended in Mg^{2+}/EGTA and Mn^{2+} than in Ca^{2+}/Mg^{2+} (Fig. S1), which is consistent with previous flow cytometric (Humphries, 2000), crystallographic (Xiong et al., 2001), and electron microscopic (Takagi et al., 2002; Zhu et al., 2008) studies. The affinity of FN–$\alpha_5\beta_1$ binding was low in Ca^{2+}/Mg^{2+} but high in Mg^{2+}/EGTA or Mn^{2+} (Mould et al., 1995), which was manifested as different adhesion frequencies (Fig. 2, A and C). At low forces (<10 pN), FN–$\alpha_5\beta_1$ bonds dissociated rapidly (lifetimes <2 s) in all three cation conditions (Fig. 3, A–C), suggesting that Mg^{2+}/EGTA or Mn^{2+} increased the on rate for association but did not significantly impact the off rate for dissociation. These are consistent with our previous kinetic measurements of integrin $\alpha_L\beta_2$ interacting from intercellular adhesion molecule 1 under these cations, which showed fast force-free off rates and a much greater responsiveness to cation conditions of on rates than off rates (Zhang et al., 2005).

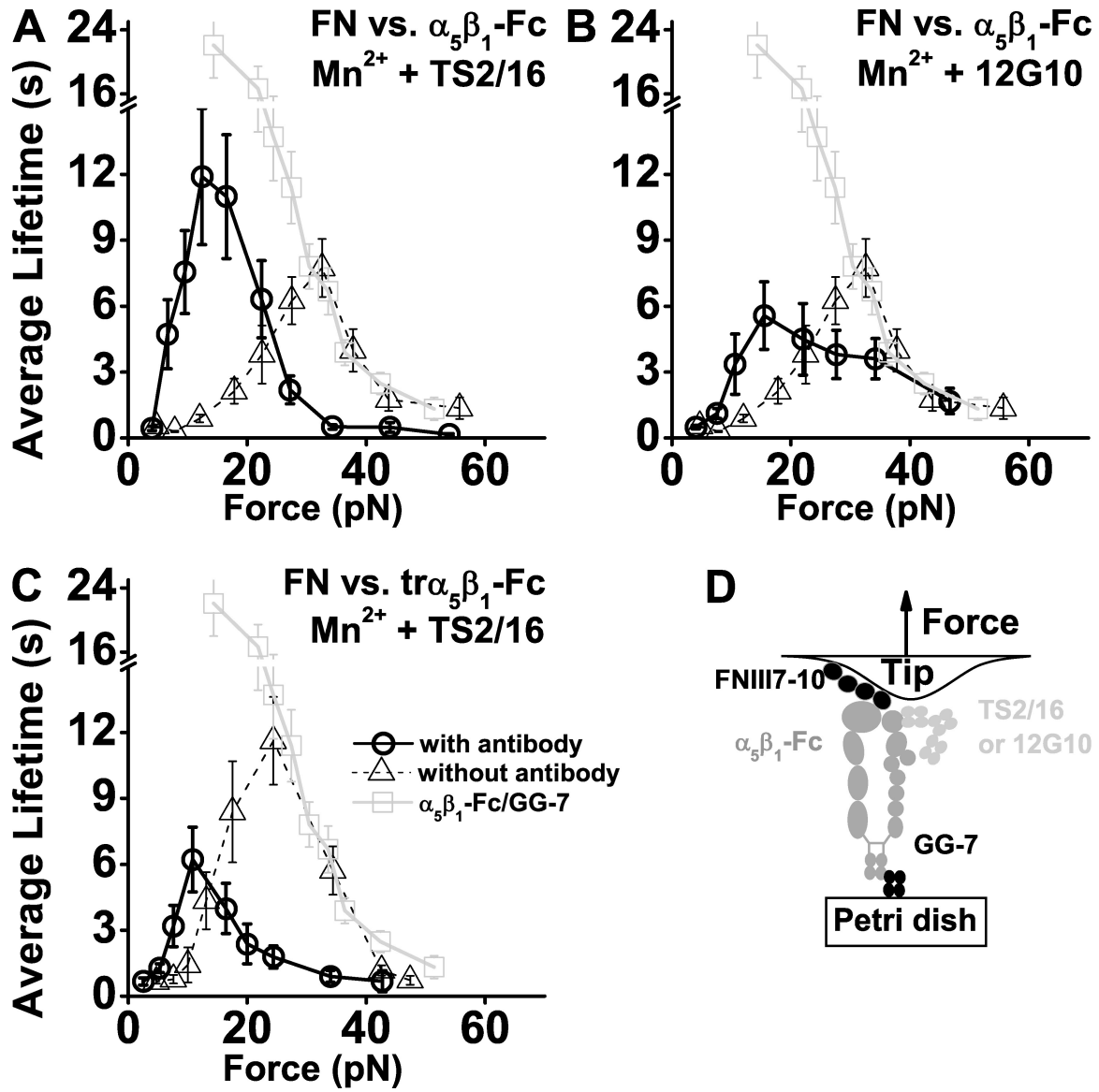

Figure 6. **Effects of activating mAbs.** (A–C) Lifetime (mean ± SEM) versus force plots (circles) of $\alpha_5\beta_1$-Fc–functionalized Petri dish dissociating from $FNIII_{7–10}$-coated cantilever tips in Mn^{2+} and 10 µg/ml TS2/16 (A) or 12G10 (B) or tr$\alpha_5\beta_1$-Fc–functionalized Petri dish dissociating from $FNIII_{7–10}$-coated cantilever tips in Mn^{2+} and 10 µg/ml TS2/16 (C). For comparison, data from Fig. 3 C are replotted in A and B, and some of the data from Fig. 5 C are replotted in C, where the lifetime versus force curves of tr$\alpha_5\beta_1$-Fc–functionalized Petri dish dissociating from $FNIII_{7–10}$-coated cantilever tips are shown as triangles, and $\alpha_5\beta_1$-Fc–coated cantilever tips dissociating from GG-7–functionalized Petri dish are shown as squares. (D) Schematic of the molecular arrangement indicating binding sites for TS2/16 and 12G10.

In previous tension-free studies, Mn^{2+} has often been considered to be able to activate integrin to a high affinity state for ligand binding (Mould et al., 1995; Takagi et al., 2002), which corresponds to the bond state at low forces in our experiment. Then, force is able to further strengthen the bond, inducing new bond states previously not identified (Friedland et al., 2009).

It has been suggested that force applied to a bent integrin may straighten it to an extended integrin, thereby giving rise to catch bonds (Chigaev et al., 2003; Zhu et al., 2005; Alon and Dustin, 2007; Luo et al., 2007; McEver and Zhu, 2007). However, catch bonds were observed not only for FN interacting with $\alpha_5\beta_1$ (Fig. 3, A–C) in three different cation conditions but also for FN interacting with tr$\alpha_5\beta_1$ that lack the leg regions (Fig. 5, A–C), which indicates that force-induced unbending is not a required conformational change for FN–$\alpha_5\beta_1$ catch bonds.

An essential feature of integrin activation is a swing of the β subunit hybrid domain away from the α subunit (Takagi et al., 2002; Mould et al., 2003a). Based on steered molecular dynamics simulations, it has been proposed that, without a lateral force to separate the integrin legs, pulling on an extended integrin would prevent the hybrid domain from swinging outwards, thereby stabilizing the inactive conformation of the headpiece (Zhu et al., 2008). However, in our experiments, no lateral force was applied to separate the integrin legs, which were restrained. Yet, pulling on $\alpha_5\beta_1$ via a bound FN prolonged bond lifetimes at low forces, indicating that force activates rather than deactivates $\alpha_5\beta_1$. It is possible that, at least in our system, the bond

strengthening caused by pulling on the α1 helix connection may outweigh the effects of force on hybrid domain movement.

Similar to the recombinant $\alpha_5\beta_1$-Fc fusion protein, native $\alpha_5\beta_1$ purified from cell membrane and reconstituted into glass-supported lipid bilayers also formed catch bonds with FN in the same force range, although the apparent lifetimes were shorter (Fig. 3 D). For the majority of the adhesion events, the shorter lifetimes may not be caused by extraction of $\alpha_5\beta_1$ from the lipid bilayer because the running adhesion frequency remained stable in a large number of repeated contacts (Fig. S4 A) and over a long period of time (Fig. S4 B), even when the same cantilever tip was used to contact the same lipid bilayer location, indicating that neither the tip nor the bilayer lost functionality over time (Chesla et al., 1998). However, it is possible that some very long lifetimes (>10 s) could be cut short by extrapolating of integrin from the bilayer. In addition, more $\alpha_5\beta_1$-Fc might be in an extended conformation than $m\alpha_5\beta_1$ in the same cation condition, resulting in longer lifetimes for the catch bonds of FN with $\alpha_5\beta_1$-Fc than with $m\alpha_5\beta_1$ (Mould et al., 2005). As discussed in the preceding paragraph, in the bent conformation, bond lifetimes were less prolonged in the catch regime. Although catch bonds were observed for both interactions of FN with $\alpha_5\beta_1$-Fc and $m\alpha_5\beta_1$, the causes of their lifetime differences remain unclear and require further studies.

Binding of TS2/16 or 12G10 left shifted the FN–$tr\alpha_5\beta_1$-Fc catch bond region by prolonging lifetimes at low forces (Fig. 6, A–C). Both mAbs bind at or near to the α1 helix of the βA domain (Fig. 6 D; Mould et al., 2002), suggesting that this region could be important in regulating the catch bond behavior.

In addition to the RGD-binding site at the βA domain of the β_1 subunit, the β propeller of the α_5 subunit may bind the synergy site at the $FNIII_9$ domain to strengthen the FN–$\alpha_5\beta_1$ interaction (Garcia et al., 2002; Mould et al., 2003b; Friedland et al., 2009). It has recently been proposed that the FN–$\alpha_5\beta_1$ bond can be switched from a relaxed to the tensioned states in response to mechanical force through engaging the synergy site in FN (Friedland et al., 2009). Multiple sites have also been proposed for ligand binding to integrin headpieces (Hynes, 2002; Liddington and Ginsberg, 2002; Friedland et al., 2009). Thus, FN–$\alpha_5\beta_1$ catch bonds could also involve force-induced binding of multiple sites that strengthen the molecular complex.

Interestingly, the natural log (number of measurements with a lifetime >*t*) versus *t* plots for the FN–$\alpha_5\beta_1$-Fc bond exhibited multiple line segments (Fig. S5, A–C), which are in contrast to the more linear plots of the $\alpha_5\beta_1$-Fc–GG-7 bond (Fig. S5 D). The negative slope of a line reflects the off rate of the subpopulation of dissociation events associated with that line (Marshall et al., 2003). Multiple line segments suggest multiple states of single FN–$\alpha_5\beta_1$-Fc bonds rather than multiple FN–$\alpha_5\beta_1$-Fc bonds because $\alpha_5\beta_1$-Fc were captured by GG-7 Fab randomly and sparsely adsorbed and because the lifetimes were measured from single rupture events. Similar multiple-bond states were observed for FimH–mannose catch bonds (Thomas et al., 2006). These are different from the selectin–ligand catch bonds that show single lines in such plots (Marshall et al., 2003; Sarangapani et al., 2004). Instead of the aforementioned allosteric, multisite, and multistate models, a sliding rebinding model was proposed for selectin–ligand (Lou et al., 2006; Lou and Zhu, 2007) and GPIbα–VWF (Yago et al., 2008) catch bonds. These mechanisms are not mutually exclusive and may work together to give rise to integrin–ligand catch bonds.

As cell adhesion molecules, integrins function as mechanical connectors. They also transduce signals bidirectionally from inside out and from outside in across the cell membrane. Such a dual role makes integrins prime candidates for force-sensing molecules in mechanotransduction (Schwartz and DeSimone, 2008). Catch bonds provide a physical mechanism for force sensing if different bond lifetimes correspond to different activation states that transduce distinct signals. The ability of integrin–ligand bonds to be strengthened by force may be of great importance not only for leukocyte trafficking, which occurs under hydrodynamic forces, but also for the migration of many other cell types, which involves cyclic adhesion and detachment between the cell and the ECM. Catch bonds may provide a mechanical mechanism for the cell to regulate adhesion by applying different forces at different times and locations when and where different adhesion strengths are desired.

Materials and methods

Recombinant $\alpha_5\beta_1$-Fc and $tr\alpha_5\beta_1$-Fc chimeras were generated by CHOL761h cells that were transiently transfected with cDNA constructs encoding the human α_5 (Fitzgerald et al., 1987) and β_1 (Coe et al., 2001) subunits or $tr\alpha_5$ and $tr\beta_1$ subunits (Coe et al., 2001). Purified $m\alpha_5\beta_1$ was obtained from Millipore. $FNIII_{7–10}$ with a biotin tag at the N terminus was produced using standard recombinant DNA techniques (Petrie et al., 2006). Anti-$\alpha_5\beta_1$–blocking (P1D6) and –activating (TS2/16) mAbs were obtained from Millipore, reporting mAb (9EG7) was obtained from BD, and another activating mAb (12G10) was obtained from Abcam. The anti-FN mAb (HFN7.1) was obtained from Developmental Studies Hybridoma Bank. The anti–human Fc-capturing mAb (GG-7) was obtained from Sigma-Aldrich.

The AFM is a modification of a previously described system (Marshall et al., 2003; Sarangapani et al., 2004) built and calibrated in house. It consists of a PZT on which a Petri dish is directly mounted (Fig. 1 A). The PZT has a capacitive feedback control that gives subnanometer position resolution. A laser (Oz Optics) focused on the end of the cantilever (TM microscopes) is deflected onto a photodiode (Hamamatsu Photonics) to measure cantilever deflection, which is converted to force using the cantilever spring constant. Spring constant (3–12 pN/nm) for each cantilever was calibrated in situ using thermal fluctuation analysis (Hutter and Bechhoefer, 1993). A personal computer with a data acquisition board (National Instruments) was used to control movements of the PZT and to collect signals from the photodiode. Labview (National Instruments) was used as the interface between the user and the data acquisition board.

To measure the interaction of $\alpha_5\beta_1$-Fc or $tr\alpha_5\beta_1$-Fc with $FNIII_{7–10}$ (Fig. 3 E and Fig. 5 D) or $\alpha_5\beta_1$-Fc with P1D6 (Fig. 4 A, schematic), cantilever tips were incubated with 10–20 µg/ml $FNIII_{7–10}$ or P1D6 overnight at 4°C (Fig. 1 B). After rinsing with TBS (25 mM Tris-HCl and 150 mM NaCl, pH 7.4), the cantilevers were incubated for 15 min at room temperature in TBS containing 1% BSA to block nonspecific adhesion. GG-7 was cleaved into Fab and Fc fragments by using the Fab preparation kit following the manufacturer's instructions (Thermo Fisher Scientific). The fragmented GG-7 (at coating concentration indicated in Fig. 2) was adsorbed on a small spot on a Petri dish by overnight incubation at 4°C. To capture $tr\alpha_5\beta_1$-Fc, the GG-7–precoated Petri dish was rinsed three times with TBS and incubated with 10 µg/ml $tr\alpha_5\beta_1$-Fc at the desired cation condition (Ca^{2+}/Mg^{2+}, Mg^{2+}/EGTA, or Mn^{2+}) for 30 min. The Petri dish was again rinsed three times with TBS and filled with 5 ml TBS plus 1% BSA and the indicated cations. In some experiments, 10 µg/ml HFN7.1, 1 mg/ml cyclo(-GRGDSP) (AnaSpec, Inc.), or 10 µg/ml TS2/16 or 12G10 (Fig. 6 D) were added to the buffer.

To measure the interaction of $FNIII_{7–10}$ with HFN7.1 (Fig. 4 B, schematic) or $\alpha_5\beta_1$-Fc with GG-7 Fab (Fig. 3 F), $FNIII_{7–10}$ or $\alpha_5\beta_1$-Fc was adsorbed on cantilevers and treated as described in the previous paragraph. 10 µg/ml

goat anti–mouse Fc polyclonal antibody or 20 µg/ml fragmented GG-7 was adsorbed on a labeled spot on a Petri dish overnight at 4°C. To capture HFN7.1, the Petri dish was rinsed three times with TBS and incubated with 10 µg/ml HFN7.1 for 30 min. The Petri dish was again rinsed three times with TBS and filled with 5 ml TBS plus 1% BSA and the indicated cations.

To measure the interaction of $FNIII_{7–10}$ with $m\alpha_5\beta_1$, cantilevers were coated with streptavidin at 50 µg/ml overnight at 4°C and further functionalized by incubation with 10 µl of 1 µg/ml $FNIII_{7–10}$ for 15 min at room temperature. $m\alpha_5\beta_1$-incoporated lipid vesicle solution was prepared according to Muller et al. (1993). In brief, vesicles were formed by hydrating a dried lipid film of 1,2-dimyristoyl-*sn*-glycero-3-phosphocholine and 1,2-dimyristoyl-*sn*-glycero-3-[phospho-*rac*-(1-glycerol)] (Avanti Polar Lipids, Inc.) in a 50:50 ratio with 0.1% Triton X-100 (Thermo Fisher Scientific) in TBS and mixed with $m\alpha_5\beta_1$, resulting in a final concentration of 0.27 mg/ml (0.4 mM) of lipid and 0.1 mg/ml of integrin. Triton X-100 was removed by adsorption to Bio-Beads SM-2 (Bio-Rad Laboratories, Inc.) at 37°C for 4 h. The resulting lipid vesicle solution was stored under argon at 4°C and used within several months. Coverslips of 40 mm in diameter (Bioptechs) were cleaned with a mixture of 70% 12 N sulfuric acid and 30% hydrogen peroxide by volume at 100°C for 45 min, rinsed extensively with deionized water, and dried completely under an argon stream. The cleaned coverslip, which was used immediately, was placed in a Petri dish, and a 4-µl drop of $m\alpha_5\beta_1$-incorporated lipid vesicle solution was placed on the coverslip surface. After 20 min of incubation under a damp paper towel, the Petri dish was filled with 5 ml TBS with 2 mM Mg^{2+}, 2 mM EGTA, and 1% BSA. The $m\alpha_5\beta_1$ bilayers that formed had low molecular densities to ensure their infrequent binding to the $FNIII_{7–10}$-coated cantilever tips, as required for measuring single bonds. Bilayers were immediately used in AFM experiments.

The AFM force-clamp experiments were performed by repeatedly bringing the Petri dish in contact with the cantilever tip, then immediately retracting a small distance (0–5 nm), holding at that distance for 0.5 s to allow bond formation, and retracting again at a speed of 200 nm/s. By preventing the cantilever tip from compressing the Petri dish during the time for molecular association, the nonspecific binding was greatly suppressed (Fig. 2; and Fig. S2, B–D). The presence of adhesion was detected from the force-scan curves (Fig. 1, C and D). A feedback system was used to clamp the force at a desired level to enable measurement of bond lifetime at constant force. Approximately 50 lifetimes were measured in the full-force range (5–70 pN) using a cantilever and a Petri dish in each experiment. Measurements from all of the experiments were pooled and binned. For example, for FN–$\alpha_5\beta_1$-Fc–GG-7 interaction in 1 mM Ca^{2+}/Mg^{2+} condition, 13 experiments were performed to acquire 846 lifetimes at forces ranging from 5–70 pN. These were segregated into 12 force bins, each of which spanned 5–6 pN and contained at least ~50 lifetimes. Lifetimes were plotted versus force as mean ± SEM in Figs. 3–6. Plots of natural log (number of events with a lifetime >*t*) versus *t* were exemplified for the FN–$\alpha_5\beta_1$-Fc–GG-7 bond in the three cation conditions (Fig. S5, A–C) and for the $\alpha_5\beta_1$-Fc–GG-7 bond (Fig. S5 D).

Binding of 9EG7 to $\alpha_5\beta_1$-Fc in different divalent cations was determined by flow cytometry. 125 µg (50 µl) streptavidin-coated magnetic beads (Thermo Fisher Scientific) were incubated with GG-7 biotinylated using BiotinTag micro biotinylation kit (Sigma-Aldrich) in 1 ml PBS at a concentration of 5 µg/ml for 30 min. 40 µl beads were washed three times in TBS, incubated with 20 µg/ml $\alpha_5\beta_1$-Fc in 200 ml TBS with desired cations for 30 min, again washed three times in TBS with appropriate cations, and incubated with 9EG7 at 10 µg/ml for 30 min. 9EG7 was preconjugated with allophycocyanin using the lightning-link APC-XL conjugation kit following the manufacturer's instructions (Innova Bioscience). After washing three times with TBS containing the appropriate cations, beads were analyzed by flow cytometry.

Online supplemental material

Fig. S1 shows flow cytometry analysis of the expression of 9EG7 epitope by $\alpha_5\beta_1$-Fc in different cation conditions. Fig. S2 demonstrates histograms of rupture forces and additional controls for binding specificity. Fig. S3 demonstrates lack of correlation between bond lifetime and molecular stiffness. Fig. S4 demonstrates functional stability of $\alpha_5\beta_1$ in supported lipid bilayer. Fig. S5 shows lifetime distributions. Online supplemental material is available at http://www.jcb.org/cgi/content/full/jcb.200810002/DC1.

We thank T.A. Petrie for production of $FNIII_{7–10}$ and R.P. McEver for reading the manuscript.

This work was supported by National Institutes of Health grants AI60799 and AI44902 (to C. Zhu) and GM065918 (to A.J. García).

Submitted: 1 October 2008
Accepted: 1 June 2009

References

Akiyama, S.K., S.S. Yamada, W.T. Chen, and K.M. Yamada. 1989. Analysis of fibronectin receptor function with monoclonal antibodies: roles in cell adhesion, migration, matrix assembly, and cytoskeletal organization. *J. Cell Biol.* 109:863–875.

Alon, R., and M.L. Dustin. 2007. Force as a facilitator of integrin conformational changes during leukocyte arrest on blood vessels and antigen-presenting cells. *Immunity.* 26:17–27.

Astrof, N.S., A. Salas, M. Shimaoka, J. Chen, and T.A. Springer. 2006. Importance of force linkage in mechanochemistry of adhesion receptors. *Biochemistry.* 45:15020–15028.

Bell, G.I. 1978. Models for the specific adhesion of cells to cells. *Science.* 200:618–627.

Chesla, S.E., P. Selvaraj, and C. Zhu. 1998. Measuring two-dimensional receptor-ligand binding kinetics by micropipette. *Biophys. J.* 75:1553–1572.

Chigaev, A., T. Buranda, D.C. Dwyer, E.R. Prossnitz, and L.A. Sklar. 2003. FRET detection of cellular α4-integrin conformational activation. *Biophys. J.* 85:3951–3962.

Coe, A.P.F., J.A. Askari, A.D. Kline, M.K. Robinson, H. Kirby, P.E. Stephens, and M.J. Humphries. 2001. Generation of a minimal $\alpha_5\beta_1$ integrin-Fc fragment. *J. Biol. Chem.* 276:35854–35866.

Dembo, M., D.C. Torney, K. Saxman, and D. Hammer. 1988. The reaction-limited kinetics of membrane-to-surface adhesion and detachment. *Proc. R. Soc. Lond. B. Biol. Sci.* 234:55–83.

Fitzgerald, L.A., M. Poncz, B. Steiner, S.C. Rall Jr., J.S. Bennett, and D.R. Phillips. 1987. Comparison of cDNA-derived protein sequences of the human fibronectin and vitronectin receptor alpha-subunits and platelet glycoprotein IIb. *Biochemistry.* 26:8158–8165.

Friedland, J.C., M.H. Lee, and D. Boettiger. 2009. Mechanically activated integrin switch controls alpha5beta1 function. *Science.* 323:642–644.

Galbraith, C.G., K.M. Yamada, and M.P. Sheetz. 2002. The relationship between force and focal complex development. *J. Cell Biol.* 159:695–705.

Garcia, A.J., M.D. Vega, and D. Boettiger. 1999. Modulation of cell proliferation and differentiation through substrate-dependent changes in fibronectin conformation. *Mol. Biol. Cell.* 10:785–798.

Garcia, A.J., J.E. Schwarzbauer, and D. Boettiger. 2002. Distinct activation states of $\alpha_5\beta_1$ integrin show differential binding to RGD and synergy domains of fibronectin. *Biochemistry.* 41:9063–9069.

Guo, B., and W.H. Guilford. 2006. Mechanics of actomyosin bonds in different nucleotide states are tuned to muscle contraction. *Proc. Natl. Acad. Sci. USA.* 103:9844–9849.

Humphries, M.J. 2000. Integrin structure. *Biochem. Soc. Trans.* 28:311–339.

Hutter, J.L., and J. Bechhoefer. 1993. Calibration of atomic-force microscope tips. *Rev. Sci. Instrum.* 64:1868–1873.

Hynes, R.O. 2002. Integrins: bidirectional, allosteric signaling machines. *Cell.* 110:673–687.

Jin, M., I. Andricioaei, and T.A. Springer. 2004. Conversion between three conformational states of integrin I domains with a C-terminal pull spring studied with molecular dynamics. *Structure.* 12:2137–2147.

Li, F., S.D. Redick, H.P. Erickson, and V.T. Moy. 2003. Force measurements of the α5β1 integrin-fibronectin interaction. *Biophys. J.* 84:1252–1262.

Liddington, R.C., and M.H. Ginsberg. 2002. Integrin activation takes shape. *J. Cell Biol.* 158:833–839.

Luo, B.H., C.V. Carman, and T.A. Springer. 2007. Structural basis of integrin regulation and signaling. *Annu. Rev. Immunol.* 25:619–647.

Lou, J., and C. Zhu. 2007. A structure-based sliding-rebinding mechanism for catch bonds. *Biophys. J.* 92:1471–1485.

Lou, J., T. Yago, A.G. Klopocki, P. Mehta, W. Chen, V.I. Zarnitsyna, N.V. Bovin, C. Zhu, and R.P. McEver. 2006. Flow-enhanced adhesion regulated by a selectin interdomain hinge. *J. Cell Biol.* 174:1107–1117.

Marshall, B.T., M. Long, J.W. Piper, T. Yago, R.P. McEver, and C. Zhu. 2003. Direct observation of catch bonds involving cell-adhesion molecules. *Nature.* 423:190–193.

McEver, R.P., and C. Zhu. 2007. A catch to integrin activation. *Nat. Immunol.* 8:1035–1037.

Mould, A.P., S.K. Akiyama, and M.J. Humphries. 1995. Regulation of integrin α5β1-fibronectin interactions by divalent cations. *J. Biol. Chem.* 270:26270–26277.

Mould, A.P., J.A. Askari, S. Barton, A.D. Kline, P.A. McEwan, S.E. Craig, and M.J. Humphries. 2002. Integrin activation involves a conformational change in the α1 helix of the β subunit A-domain. *J. Biol. Chem.* 277:19800–19805.

Mould, A.P., S.J. Barton, J.A. Askari, P.A. McEwan, P.A. Buckley, S.E. Craig, and M.J. Humphries. 2003a. Conformational changes in the integrin beta

A domain provide a mechanism for signal transduction via hybrid domain movement. *J. Biol. Chem.* 278:17028–17035.

Mould, A.P., E.J.H. Symonds, P.A. Buckley, J.G. Grossmann, P.A. McEwan, S.J. Barton, J.A. Askari, S.E. Craig, J. Bella, and M.J. Humphries. 2003b. Structure of an integrin-ligand complex deduced from solution x-ray scattering and site-directed mutagenesis. *J. Biol. Chem.* 278:39993–39999.

Mould, A.P., M.A. Travis, S.J. Barton, J.A. Hamilton, J.A. Askari, S.E. Craig, P.R. MacDonald, R.A. Kammerer, P.A. Buckley, and M.J. Humphries. 2005. Evidence that monoclonal antibodies directed against the integrin β subunit plexin/semaphorin/integrin domain stimulate function by inducing receptor extension. *J. Biol. Chem.* 280:4238–4246.

Muller, B., H.G. Zerwes, K. Tangemann, J. Peter, and J. Engel. 1993. Two-step binding mechanism of fibrinogen to αIIbß3 integrin reconstituted into planar lipid bilayers. *J. Biol. Chem.* 268:6800–6808.

Petrie, T.A., J.R. Capadona, C.D. Reyes, and A.J. Garcia. 2006. Integrin specificity and enhanced cellular activities associated with surfaces presenting a recombinant fibronectin fragment compared to RGD supports. *Biomaterials.* 27:5459–5470.

Puklin-Faucher, E., M. Gao, K. Schulten, and V. Vogel. 2006. How the headpiece hinge angle is opened: new insights into the dynamics of integrin activation. *J. Cell Biol.* 175:349–360.

Rief, M., M. Gautel, F. Oesterhelt, J.M. Fernandez, and H.E. Gaub. 1997. Reversible unfolding of individual titin immunoglobulin domains by AFM. *Science.* 276:1109–1112.

Sarangapani, K.K. 2005. Characterizing selectin-ligand bonds using atomic force microscopy (AFM). PhD dissertation. Georgia Institute of Technology, Atlanta, GA. 90 pp.

Sarangapani, K.K., T. Yago, A.G. Klopocki, M.B. Lawrence, C.B. Fieger, S.D. Rosen, R.P. McEver, and C. Zhu. 2004. Low force decelerates L-selectin dissociation from P-selectin glycoprotein ligand-1 and endoglycan. *J. Biol. Chem.* 279:2291–2298.

Schwartz, M.A., and D.W. DeSimone. 2008. Cell adhesion receptors in mechanotransduction. *Curr. Opin. Cell Biol.* 20:551–556.

Shimizu, Y., G.A.V. Seventer, K.J. Horgan, and S. Shaw. 1990. Regulated expression and binding of three VLA (β1) integrin receptors on T cells. *Nature.* 345:250–253.

Takagi, J., B.M. Petre, T. Walz, and T.A. Springer. 2002. Global conformational rearrangements in integrin extracellular domains in outside-in and inside-out signaling. *Cell.* 110:599–611.

Thomas, W., M. Forero, O. Yakovenko, L. Nilsson, P. Vicini, E. Sokurenko, and V. Vogel. 2006. Catch-bond model derived from allostery explains force-activated bacterial adhesion. *Biophys. J.* 90:753–764.

Vitte, J., A. Pierres, A.-M. Benoliel, and P. Bongrand. 2004. Direct quantification of the modulation of interaction between cell- or surface-bound LFA-1 and ICAM-1. *J. Leukoc. Biol.* 76:594–602.

Woolf, E., I. Grigorova, A. Sagiv, V. Grabovsky, S.-W. Feigelson, Z. Shulman, T. Hartmann, M. Sixt, J.-G. Cyster, and R. Alon. 2007. Lymph node chemokines promote sustained T lymphocyte motility without triggering stable integrin adhesiveness in the absence of shear forces. *Nat. Immunol.* 8:1076–1085.

Xiao, T., J. Takagi, B.S. Coller, J.H. Wang, and T.A. Springer. 2004. Structural basis for allostery in integrins and binding to fibrinogen-mimetic therapeutics. *Nature.* 432:59–67.

Xiong, J.P., T. Stehle, B. Diefenbach, R. Zhang, R. Dunker, D.L. Scott, A. Joachimiak, S.L. Goodman, and M.A. Arnaout. 2001. Crystal structure of the extracellular segment of integrin αVβ3. *Science.* 294:339–345.

Yago, T., J. Lou, T. Wu, J. Yang, J.J. Miner, L. Coburn, J.A. Lopez, M.A. Cruz, J.F. Dong, L.V. McIntire, et al. 2008. Platelet glycoprotein Ibα forms catch bonds with human WT vWF but not with type 2B von Willebrand disease vWF. *J. Clin. Invest.* 118:3195–3207.

Yakovenko, O., S. Sharma, M. Forero, V. Tchesnokova, P. Aprikian, B. Kidd, A. Mach, V. Vogel, E. Sokurenko, and W.-E. Thomas. 2008. FimH forms catch bonds that are enhanced by mechanical force due to allosteric regulation. *J. Biol. Chem.* 283:11596–11605.

Zhang, F., W.D. Marcus, N.-H. Goyal, P. Selvaraj, T.A. Springer, and C. Zhu. 2005. Two-dimensional kinetics regulation of $\alpha_L\beta_2$-ICAM-1 interaction by conformational changes of the αL-inserted domain. *J. Biol. Chem.* 280:42207–42218.

Zhang, X., E. Wojcikiewicz, and V.T. Moy. 2002. Force spectroscopy of the leukocyte function-associated antigen-1/intercellular adhesion molecule-1 interaction. *Biophys. J.* 83:2270–2279.

Zhang, X., S.E. Craig, H. Kirby, M.J. Humphries, and V.T. Moy. 2004. Molecular basis for the dynamic strength of the integrin $\alpha_4\beta_1$/VCAM-1 interaction. *Biophys. J.* 87:3470–3478.

Zhu, C., J.Z. Lou, and R.P. McEver. 2005. Catch bonds: physical models, structural bases, biological function and rheological relevance. *Biorheology.* 42:443–462.

Zhu, J., B.H. Luo, T. Xiao, C. Zhang, N. Nishida, and T.A. Springer. 2008. Structure of a complete integrin ectodomain in a physiologic resting state and activation and deactivation by applied forces. *Mol. Cell.* 32:849–861.